Respiratory Syncytial Virus NS1 Protein Targets the Transactivator Binding Domain of MED25

Jiawei Dong, Vincent Basse, Maxime Bierre, Andressa Peres de Oliveira, Pierre-Olivier Vidalain, Pierre Sibille, Frederic Tangy, Marie Galloux, Jean-Francois Eleouet, Christina Sizun, et al.

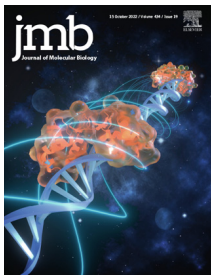

Respiratory Syncytial Virus NS1 Protein Targets the Transactivator Binding Domain of MED25

Jiawei Dong [2†], Vincent Basse [1†], Maxime Bierre [1], Andressa Peres de Oliveira [3], Pierre-Olivier Vidalain [3,4], Pierre Sibille [1], Frederic Tangy [3], Marie Galloux [1], Jean-Francois Eleouet [1], Christina Sizun [2*] and Monika Bajorek [1*]

*1 - **Université Paris-Saclay,** INRAE, UVSQ, VIM, 78350 Jouy-en-Josas, France*
*2 - **Institut de Chimie des Substances Naturelles,** CNRS UPR 2301, Université Paris-Saclay, 1 Avenue de la Terrasse, 91190 Gif-sur-Yvette, France*
*3 - **Unité de Génomique Virale et Vaccination,** Institut Pasteur, CNRS UMR 3569, 75015 Paris, France*
*4 - **CIRI,** Centre International de Recherche en Infectiologie, Univ Lyon, Inserm U1111, Université Claude Bernard Lyon 1, CNRS, UMR5308, ENS de Lyon, 69007 Lyon, France*

***Correspondence to Christina Sizun and Monika Bajorek:** christina.sizun@cnrs.fr (C. Sizun), monika.bajorek@inrae.fr (M. Bajorek) @VidalainPO (P.-O. Vidalain)*
https://doi.org/10.1016/j.jmb.2022.167763
Edited by M.F. Summers

Abstract

Human RSV is the leading cause of infantile bronchiolitis in the world and one of the major causes of childhood deaths in resource-poor settings. It is a major unmet target for vaccines and anti-viral drugs. Respiratory syncytial virus has evolved a unique strategy to evade host immune response by coding for two non-structural proteins NS1 and NS2. Recently it was shown that in infected cells, nuclear NS1 could be involved in transcription regulation of host genes linked to innate immune response, via interactions with chromatin and the Mediator complex. Here we identified the MED25 Mediator subunit as an NS1 interactor in a yeast two-hybrid screen. We demonstrate that NS1 directly interacts with MED25 *in vitro* and *in cellula,* and that this interaction involves the MED25 transactivator binding ACID domain on the one hand, and the C-terminal α3 helix of NS1, with an additional contribution of the globular domain of NS1, on the other hand. By NMR we show that the NS1 α3 sequence primarily binds to the MED25 ACID H2 face, similarly to the α-helical transactivation domains (TADs) of transcription regulators such as *Herpex simplex* VP16 and ATF6α, a master regulator of ER stress response activated upon viral infection. Moreover, we found out that the NS1 could compete with ATF6α TAD for binding to MED25. These findings point to a mechanism of NS1 interfering with innate immune response by impairing recruitment by cellular TADs of the Mediator via MED25 and hence transcription of specific genes by RNA polymerase II.

Introduction

Human RSV (hRSV) is the most frequent cause of infantile bronchiolitis and pneumonia worldwide.[1] In 2015 RSV was estimated to have caused 33.1 million episodes of acute lower respiratory infections (ALRI) in young children, resulting in 3.2 million hospital admissions and 59,600–118,200 in-hospital deaths of children younger than 5 years, worldwide.[2] Other sources estimated the number of RSV-caused ALRI episodes to be ~25 million and the death toll for

children younger than 5 years to be 41,000 in 2016.[3] The importance of RSV-associated pulmonary disease and mortality in elderly persons has also been recognized.[4] Similarly, bovine RSV (bRSV) affects cattle farms and leads to economic loss due to high morbidity and mortality among calves.[5,6] Importantly, there is still no licensed vaccine for human RSV despite over six decades of attempts,[7] emphasizing the need for a better understanding of RSV pathogenesis, and more particularly of the mechanisms that were developed by the virus to evade host innate immune responses.

The pathology associated with RSV infection results from both viral replication and the host immune response mediated first by the production of type I interferons (IFN-I), which induces the transcription of IFN-stimulating genes (ISG) and the production of proinflammatory mediators.[8,9] However, upon infection by RSV, IFN levels remain surprisingly low. This poor induction of IFN is attributed at least in part to the two RSV non-structural proteins, NS1 and NS2. NS1 and NS2 are unique to the *Orthopneumovirus* genus of the *Pneumoviridae* family, *Mononegavirales* order. They diverge among the different viruses of this genus and appear to contribute to host-range restrictions.[6,10,11] Both NS1 and NS2 also act as IFN antagonists, and many of their cytosolic targets have been identified.[12–14] As an example, NS1 inhibits RIG-I activity by interacting with MAVS as well as with TRIM25, the E3 ubiquitin ligase of RIG-I.[15,16] NS1 and NS2 were reported to localize to the mitochondria,[17] where they form a viral degradosome, leading to degradation of multiple target proteins, notably involved in type I IFN pathway.[12] NS1 was found in the cytosol as well as in the nucleus, where it is expected to interfere with host gene expression.[17,18] In a very recent publication, NS1 was shown to associate with chromatin in promotor and enhancer regions of genes related to innate immune response to viral infection.[18] By targeting these DNA regulatory regions, NS1 was suggested to suppress transcription of these genes, thus antagonizing the immune response.[18] However, the exact molecular mechanism of this suppression is not well defined yet. Further study of NS1 interaction with nuclear host factors will enable a better understanding of how RSV modulates host transcription.

Based on comparison of X-ray crystallographic structures, hRSV NS1 was proposed to be a structural paralog of the hRSV matrix (M) protein.[19–21] NS1 displays striking structural similarity with the N-terminal domain of the M protein, as both contain a 7-stranded β-sandwich clamped by an α-helix (α,β-core in Figure 1(A)). In contrast to M, NS1 lacks a second similar C-terminal domain but contains an additional C-terminal α-helix, α3 (Figure 1(A)). NS1 α3 helix was specifically shown to be involved in the modulation of host responses.[20] Mutations in the NS1 α3 helix negatively affected the transcriptional regulation of genes involved in key signalling pathways such as IFN induction and oxidative stress, resulting in 2-fold reduction of RSV replication.[20]

Two different interactome studies of RSV NS1 pointed to an interaction of NS1 with the Mediator complex.[18,22] The Mediator complex is a nuclear multi-subunit complex that is part of the preinitiation complex required for RNA polymerase II transcription, and is a known regulator of many innate immune response genes.[23–25] Several Mediator subunits were identified as potential interactors of NS1, among which MED25,[18,22] but no direct interaction was shown so far. MED25 was shown to be targeted by viral activator proteins, such as Herpes simplex virus transactivator protein VP16, which activates viral immediate-early genes during infection.[26,27] MED25 contains two folded domains: the N-terminal von Willebrand domain (residues 15–216, VWD) and the central Activator Interacting Domain (residues 392–543, ACID) (Figure 1(B)). The interdomain and C-terminal regions are predicted to be highly disordered. A cryo-EM structure of the entire mammalian Mediator complex confirmed the location of MED25 in the tail module, with VWD well integrated in the tail[28] and ACID extending outside of the complex. The ACID structure was first solved by NMR and shown to be the target of the two transactivation domains (TADs) of VP16.[26,29,30] MED25 ACID has two opposite faces, termed H2 and H1, which are both binding sites for TADs. The H1 face is targeted by the TAD of the ETS family transcription factor ERM.[30,31] The H2 face is the binding site for the second TAD of VP16, called H2 or TAD2, as well as for TADs of several other transcription regulators including p53.[29,30,32–34] VP16 TAD2 can also bind to the H1 face, although with low affinity.[32]

The putative interaction between NS1 and Mediator complex suggested by interactome studies has not been investigated in detail so far. After identifying MED25 as an NS1 interactor in a yeast two-hybrid screen, we demonstrate here that NS1 directly interacts with the MED25 ACID domain in cells. We found that the α3 helix is essential for binding to MED25 ACID, but that the NS1 α,β-core domain also presents affinity for MED25 ACID. It is noteworthy that NS1 α3 residues critical for this interaction were reported to be critical for innate immune response gene regulation.[18] By investigating more specifically the interaction between NS1 α3 and MED25 we found out that NS1 α3 preferentially targets the MED25 ACID H2 face. Moreover, we revealed that NS1 could compete with the TAD of ATF6α, involved in the innate immune response to viral infections. In contrast to transcription regulators like VP16, the small NS1 protein does not appear to have a distinct DNA-binding domain, and no specific DNA-binding region has been identified yet. Altogether, our results thus strongly suggest that NS1 could

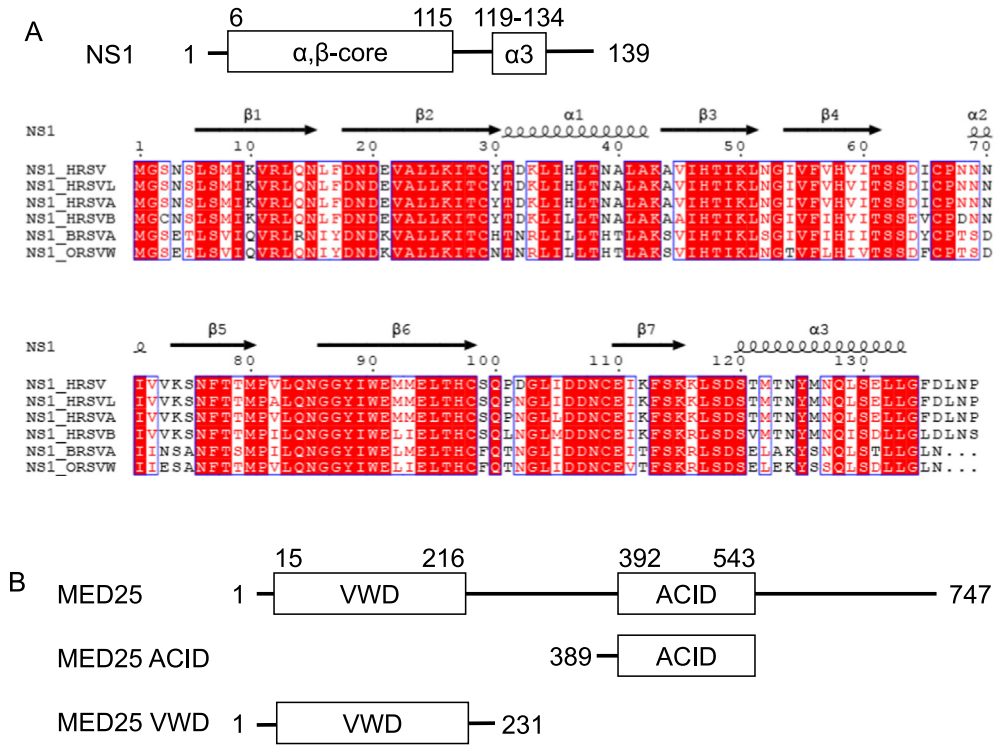

Figure 1. Representation of hRSV NS1 and MED25 structural organisation. (A) Structural organization of hRSV NS1 protein, which displays an α,β-core domain and a C-terminal α3 helix. Sequence alignment of *Orthopneumovirus* NS1 proteins: hRSV NS1 construct used in the present study, human RSV A (Uniprot P0DOE9), B (O42083) and Long (Q86306) strains, bovine RSV (Q65694) and ovine RSV (Q65703). Alignment was generated on the ClustalW server. The secondary structure elements observed in the crystallographic structure of hRSV NS1 (20) are indicated above the sequence. **(B)** Domain architecture of the Mediator subunit MED25 that contains two folded domains: the N-terminal von Willebrand domain (VWD) and the central activator interaction domain (ACID).[26,27] The boundaries of the constructs used in this study are indicated.

interfere with the host innate immune response by binding to MED25 and hindering the recruitment of transcription regulators to the Mediator, thus impairing transcription of specific host genes by RNA polymerase II.

Results

Identification of MED25 as a potential interaction partner of RSV NS1 by a yeast two-hybrid screen

To identify human proteins interacting with RSV NS1, we performed a yeast two-hybrid (Y2H) screen. The RSV NS1 protein fused with the GAL4 DNA binding domain (GAL4-BD) was expressed in yeast and used as a bait to screen two different libraries of human prey proteins fused to the GAL4 activation domain (GAL4-AD). A total of 156 positive yeast colonies were retrieved from the screen and analyzed by sequencing to identify the captured cellular preys. Following recommendations from previous reports to increase the accuracy of Y2H screens,[35,36] only interactions supported by at least three yeast colonies were considered for further analysis. This represented fifteen potential interactors of RSV NS1 and included two subunits of the human Mediator complex: MED25 and MED15 (Table 1). We chose to focus on the MED25 subunit since it was one of the most abundant interactors in our screen and was also identified in previous proteomics studies of host targets interacting with RSV NS1.[18,22] In total, 10 over 156 positive yeast colonies expressed MED25. Although six of the cDNA clones expressed full-length MED25, two started at position 261 and two others at position 308. As the four cDNA clones coding for a truncated MED25 version contained the ACID domain (Figure 1(B)), this strongly suggested a role of this domain in the interaction of MED25 with RSV NS1.

The MED25 ACID domain and the C-terminal α3 helix of NS1 interact in cells

In order to confirm the NS1-MED25 interaction found by Y2H screening, we studied whether NS1 could interact with MED25 in cells. For that purpose, we used a split-luciferase complementation assay based on the NanoLuc

Table 1 **Cellular interactors of RSV NS1 protein identified by Y2H:** number of positive yeast colonies obtained by screening two human protein libraries, a commercial spleen cDNA library and a full-length ORF library (hORFeome v3.1). Interactions supported by at least three yeast colonies were considered as hits.

Gene name	spleen cDNA library	hORFeome library	Total
PDE9A	2	35	37
KLC4	21		21
GOLGA2	16		16
MED25	**10**		**10**
MED15	8		8
SIPA1L1	8		8
HMG20A	7		7
IKBKG	6		6
CEP290	5		5
TXNDC11	5		5
RBSN	5		5
ZFYVE20	4		4
CCHCR1	3		3
NME3	3		3
RAI14	3		3

enzyme.[37] In this system, the 114 or the 11S NanoLuc fragments are fused to the C or N-terminus of each protein partner. The constructs used for this assay are shown in Figure 2(A). We used the RSV phosphoprotein (P), which is known to form tetramers,[38–43] as a positive control. Analysis of lysates of transfected 293T cells by Western blotting using anti-FLAG (for NS1 and MED25 proteins) or anti-P antibodies confirmed protein expression with the fused NanoLuc fragments (Figure 2(B)). All NS1-114 constructs were expressed at comparable amounts in cells (Figure 2(B), upper panel). 11S-MED25 and 11S-MED25 ACID were expressed, however, at different levels. In contrast, 11S-MED25 VWD expression appeared to be weak. P-114 and P-11S were expressed at comparable levels (Figure 2(B), lower panel). To investigate the NS1-MED25 interaction, combinations of two constructs were transfected into 293T cells. Cells were lysed 24 h post transfection, luciferase substrate was added, and the luminescence, which directly depends on the interaction, was measured.

As shown in Figure 2(C), co-transfection of P-114 and P-11S resulted in a high luminescence signal, indicating a strong P/P interaction, as expected. We then used the NS1/NS1 interaction as an additional control. Although the predominant form of NS1 was reported to be monomeric,[20] NS1 is also known to form dimers and higher order oligomers.[17,44] We therefore tested the NS1-114/NS1-11S pair and obtained a strong luminescence signal, revealing the capacity of NS1 to self-associate (Figure 2(C)). We then tested the interaction between RSV NS1 and full-length MED25 (Figure 2(C)). When NS1-114 was co-expressed with 11S-MED25, the luminescence signal was high, confirming the interaction in cells. We then separately tested MED25 VWD and ACID domains to identify the domain involved in NS1 interaction. Transfecting NS1-114 with 11S-MED25 ACID resulted in comparable signal to that with 11S-MED25, while transfecting NS1-114 with 11S-MED25 VWD produced only background luminescence, suggesting that MED25 ACID mediates NS1 binding. However, the contribution of MED25 VWD could not be unambiguously assessed due to weak expression (Figure 2(B)).

We next asked whether the NS1 C-terminal α3 helix could be critical for the interaction with MED25 ACID. Previously, mutations in the α3 helix were shown to negatively affect transcription of key innate immune genes.[20] We thus generated the same mutants as those in 20: three NS1 mutants with substitutions inside the α3 helix, i.e. Y125A, L132A, and L132A/L133A, and a deletion mutant Δα3, where the α3 helix was removed. Of note, the mutants Y125A and L132A/L133A were previously shown to preserve the structural integrity of NS1.[20] Luminescence was measured in cells transfected with WT or mutant NS1-114 together with 11S-MED25 ACID (Figure 2(D)). NS1 L132A/MED25 ACID co-transfection resulted in luminescence signal comparable to NS1/MED25 ACID. In contrast, co-transfection of NS1 Y125A, L132A/L133A or Δα3 with MED25 ACID significantly reduced luminescence, indicating loss of interaction. Our results with the split-NanoLuc assay thus confirmed the NS1-MED25 interaction, and allowed to identify the MED25 ACID domain and the NS1 α3 helix as interaction domains.

Last, as MED25 has been reported to localize to the nucleus,[26] and since NS1 was suggested to be actively transported to the nucleus by binding another cellular or viral protein,[18] we investigated the cellular localization of NS1. BEAS-2B cells were transfected to express FLAG-NS1 WT or mutant constructs, and the localization of NS1 protein was determined by immunofluorescence imaging after staining with anti-FLAG primary antibody (Figure 2(E)). Untagged NS1 was used as negative staining control. FLAG-NS1 localized to the nucleus and to the cytoplasm, as previously reported.[17,18] All four tested NS1 mutants localized likewise to the nucleus and to the cytoplasm, indicating that these mutations do not impair NS1 nuclear localization and are accessible to MED25.

NS1 interacts directly with MED25 ACID

Next, we investigated the interaction between human NS1 and MED25 ACID *in vitro*. We first made GST-pulldowns using recombinant proteins. GST, GST-NS1, GST-NS1 Δα3 and GST-NS1 α3 (residues 115–139) were co-expressed with MED25 ACID in *E. coli*. Bacterial lysates were incubated with glutathione beads, washed extensively and the bound complexes were analysed by SDS-PAGE and Coomassie blue

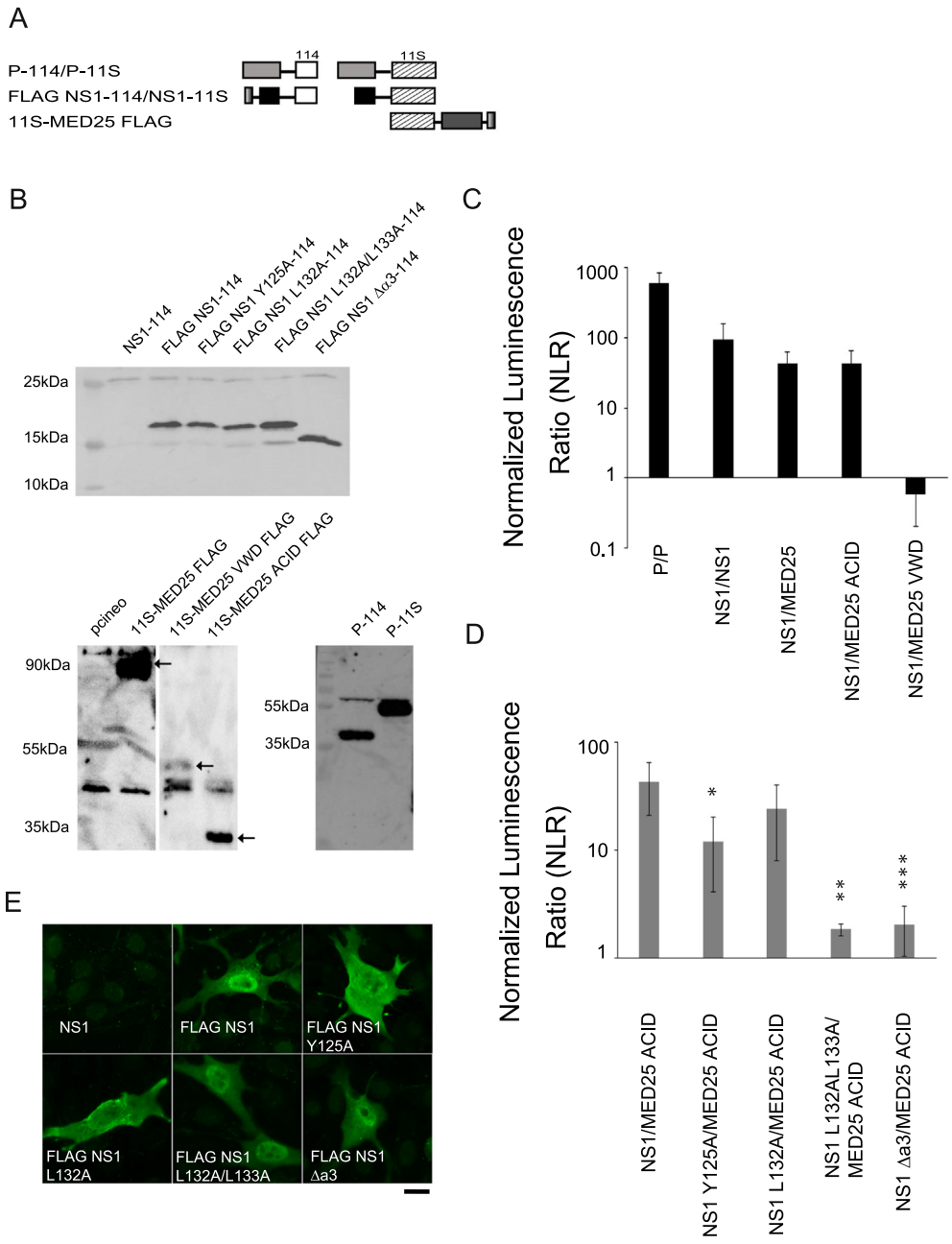

Figure 2. NS1 interacts with MED25 in cells. (A) Scheme of the protein constructs fused with NanoLUC 114 or 11S subunit used. **(B)** 293T cells were transfected with plasmids encoding NS1 or FLAG NS1 constructs fused to 114 NanoLUC, MED25 FLAG constructs fused to 11S NanoLUC, or P constructs fused to NanoLUC subunits, and cell lysates were then subjected to Western analysis using anti-FLAG or anti-P antibody. Size markers are shown on the left side of the gel. **(C, D)** MED25 and NS1 interactions were measured using the NanoLuc assay using MED25 domain deletions or using MED25 ACID and FLAG NS1 WT and α3 helix mutants. 293T cells were transfected with pairs of constructs, combined as shown in the graph. P/P and NS1/NS1 were used as positive controls. The NLR is the ratio between actual read and negative controls (each protein with the empty NanoLUC vector). The graph is representative of four independent experiments, each done in three technical repeats. Data represents the means and error bars represent standard deviation across 4 independent biological replicates. $*p < 0.05$, $**p < 0.01$, $***p < 0.001$ (unpaired two-tailed t-test). **(E)** BEAS-2B cells were transfected with plasmids encoding NS1, FLAG NS1 or FLAG NS1 mutants fused to 114 NanoLUC subunit. Cells were fixed, and immunostained with anti-FLAG (green) antibody followed by Alexa Fluor secondary antibody, and were analysed by microscopy. The scale bar represents 10 μm.

staining. As shown in Figure 3(A), MED25 ACID was pulled down by GST-NS1. MED25 ACID was also pulled down by GST-NS1 α3, confirming the interaction between the NS1 α3 helix and MED25 ACID. However, the affinity seems to be weaker than with GST-NS1. Unexpectedly, GST-NS1 Δα3 also pulled down MED25 ACID, but to a lesser extent than GST-NS1, suggesting that an additional weak interaction could take place between the α,β-core domain of NS1 and MED25 ACID.

In a second step, we measured thermodynamic binding parameters of NS1 to MED25 ACID by isothermal titration calorimetry (ITC). NS1 and MED25 ACID were produced as recombinant proteins and the GST-tag was removed from NS1. Due to the propensity of NS1 to form dimers or higher order oligomers at high concentration, we chose to titrate MED25 ACID into NS1. We used buffer and temperature conditions in which NS1 was reported to be stable.[45] The absence of oligomers was verified by dynamic light scattering (DLS) (data not shown). The ITC data show that MED25 ACID tightly binds to NS1 with a ~1:1 stoichiometry and a dissociation constant K_d of ~20 nM (Figure 3(B)). Furthermore, the interaction appears to be mainly enthalpy driven (ΔH = −11.1 kcal.mol

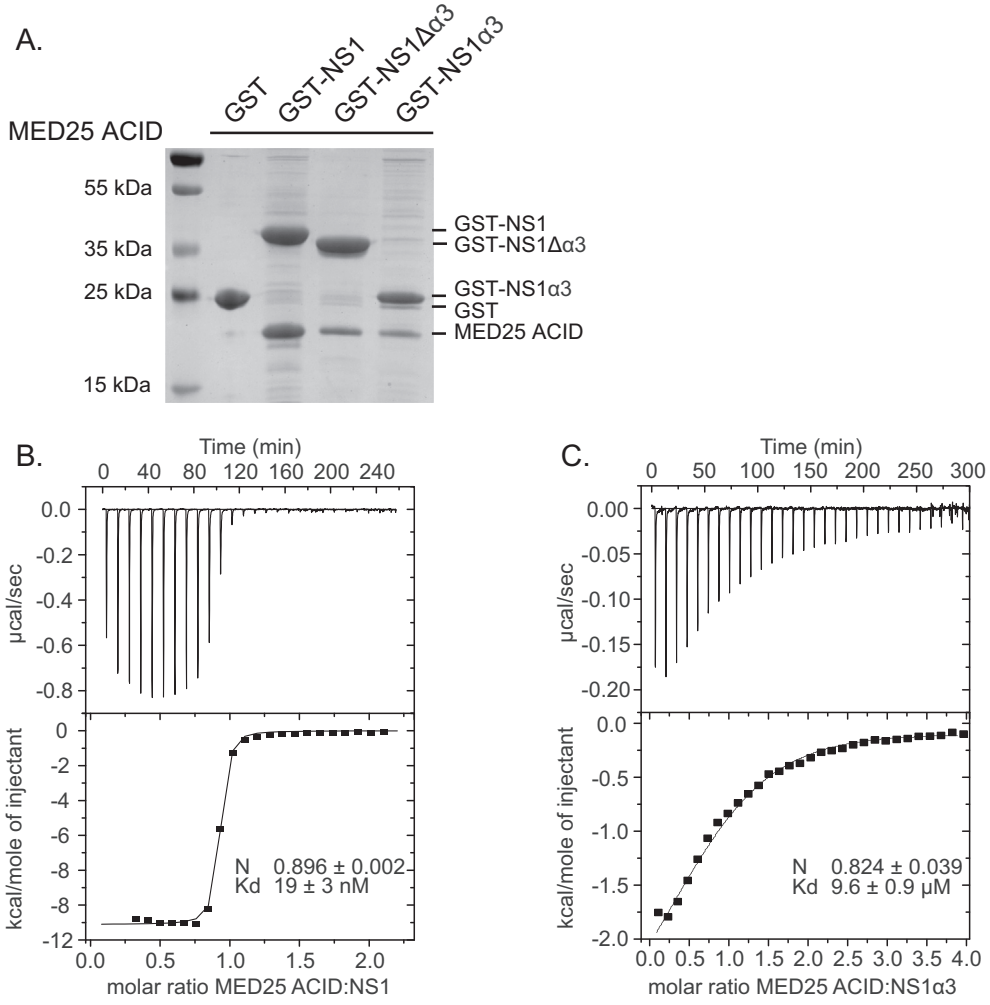

Figure 3. NS1-MED25 ACID interaction by GST pull-down assay and by isothermal titration calorimetry. (A) MED25 ACID was co-expressed together with GST, GST-NS1, GST-NS1 Δα3, or GST-NS1 α3 in *E. coli* BL21(DE3) bacteria. Bacteria lysates were clarified and the soluble protein complexes were purified on glutathione-Sepharose beads. After extensive washing the binding of MED25 ACID to GST, GST-NS1, GST-NS1 Δα3 and GST-NS1 α3 was analysed by SDS-PAGE and Coomassie blue staining. **(B) and (C)** Binding of MED25 ACID to NS1 protein and to NS1α3 peptide was measured by isothermal titration calorimetry. 300 µM MED25 ACID was titrated into 20 µM NS1, and 420 µM MED25 ACID was titrated into 20 µM NS1α3, with 8 µL injection volumes. The upper panel shows the raw heat release data after baseline correction. The lower panel shows the integrated ITC data (filled squares) fitted with a one set of sites binding model (straight line). Dissociation constants (K_d) and stoichiometric ratios (N) obtained from the fit are indicated on the lower panel.

$^{-1}$), with a small entropy penalty ($-T\Delta S$ = 0.5 kcal·mol^{-1}).

To probe the contribution of the NS1 α3 helix, we made ITC measurements with the short NS1α3 peptide (Figure 3(C)). The data were fitted with a ~1:1 stoichiometry, and the K_d was found to be 10 μM. The affinity of the NS1α3 is nearly 3 orders of magnitude lower than that of full-length NS1. This is intriguing in light of the results from split-luciferase assays in cells that show that the NS1 α3 region is critical for NS1-MED25 ACID complex formation, but corroborates the difference observed in the GST-pulldown experiments between the GST-NS1 and GST-NS1α3 constructs. A possible explanation is that the peptide corresponding to the α3 helix in the full-length NS1 does not adopt α-helical conformation, but remains unstructured. The complex formation enthalpy ΔH of −3.1 kcal·mol^{-1} is also significantly lower than with full-length NS1, suggesting that peptide solvation may contribute to the energy balance.

We thus investigated the structure of free NS1α3 peptide in solution by NMR. We recorded 1D 1H, 2D DIPSI, 2D ROESY and 2D NOESY spectra. $^{1}H_{\alpha}$ chemical shifts were close to random coil values, reporting on an unstructured peptide (Supplementary Figure 1(A)). This was corroborated by $^{3}J_{HN\text{-}H\alpha}$ scalar couplings in the 6–8 Hz range, by strong sequential H_{α}-H_N Nuclear Overhauser Effects (NOEs) in NOESY and ROESY spectra, and by NOEs between amide and water protons (Supplementary Figure 1(B–D)). On the NOESY spectrum, even with a high mixing time, we did not observe any significant sequential H_N-H_N NOEs, which would be indicative of α-helical conformation (Supplementary Figure 1 (E)). Only the C terminus, which is unstructured in the X-ray structure of NS1, and the region around Tyr125, which otherwise appeared to be unstructured, displayed weak H_N-H_N cross-peaks and hinted at some α-helical propensity. Overall these data show that the NS1α3 peptide remains unstructured. The weak affinity of the complex between MED25 ACID and NS1α3 as well as the lower capacity of GST-NS1α3 to pull down MED25 ACID, as compared to full-length NS1, may thus arise from an absence of helical conformation in the NS1α3 peptide.

Taken together, our results show that the NS1/MED25 ACID interaction is direct and of high affinity. It is mediated by the C-terminal α3 helix of NS1 in a cellular context. We evidenced a direct interaction between MED25 ACID and the NS1 α3 region *in vitro*, but the NS1 α,β-core domain also displays weak affinity.

Mapping of NS1 interaction regions on MED25 ACID by NMR

The NS1 α3 helix of NS1 reminds of the α-helical TADs that bind to MED25 ACID. We wondered whether α3 might exhibit similar binding properties. We thus performed NMR interaction experiments to map the NS1 α3 interaction site on MED25 ACID, by titrating the NS1α3 peptide into ^{15}N-labelled MED25 ACID. At each titration point we acquired a 2D ^{1}H-^{15}N HSQC spectrum (Figure 4(A)). The backbone chemical shifts of MED25 ACID were assigned *de novo* by measuring 3D triple resonance experiments on $^{15}N^{13}C$ -labelled MED25 ACID. During the titration, perturbations of individual MED25 ACID amide signals were observed, showing that the NS1α3 peptide binds to MED25 ACID (Figure 4(A)).

For most of these residues, saturation was reached at a molar peptide:protein ratio r between 1.7 and 2.3, indicating a titration endpoint. Due to the small size of the peptide, no significant line broadening was observed for the NMR signals of the complex as compared to free protein, which facilitated data analysis. Many of the perturbed signals exhibited a linear variation of chemical shifts up to saturation, indicative of a fast exchange regime on a chemical shift scale. Some residues, like Gly524, additionally exhibited line broadening during titration, indicative of a fast-to-intermediate exchange regime between free and bound forms (inset in Figure 4(A)). A few residues, like Thr460, were nearly completely broadened out at intermediate titration points. The signals of the two latter categories were recovered at r ~1.7 and 2.3, suggesting that these perturbations report on the same binding event as those in fast exchange. Moreover, they displayed large ^{1}H and/or ^{15}N chemical shift differences between free and bound forms, which is compatible with a transition from fast to intermediate exchange regime.

Combined ^{1}H and ^{15}N chemical shifts perturbations ($\Delta\delta_{HN}$ CSPs) as a function of the protein sequence were plotted in Figure 4(B) for two different molar peptide:protein ratios r = 1.1 and r = 2.3. Residues with large CSPs in a fast or fast-to-intermediate exchange regime were mapped onto the 3D structure of MED25 ACID (with 2 cut-offs in green and yellow, Figure 4(C)). These perturbations are predominantly located on the H2 face of MED25 ACID, corresponding to the binding surface of the second transactivation domain (TAD2) of VP16.[29,30,32] Residues in an intermediate exchange were also mapped onto the MED25 ACID structure (in orange, Figure 4 (C)). They also belong to the H2 face, confirming that they report on the same binding event. The area perturbed by NS1α3 extends to the junction between the H1 and H2 faces, suggesting that NS1α3 binding may be accompanied by conformational rearrangement of MED25 ACID, for example by repositioning of the C-terminal α3 helix with respect to the β-barrel (Figure 4(C)).

The affinity between the NS1α3 peptide and MED25 ACID was evaluated by determining dissociation constants (K_d) for residues with

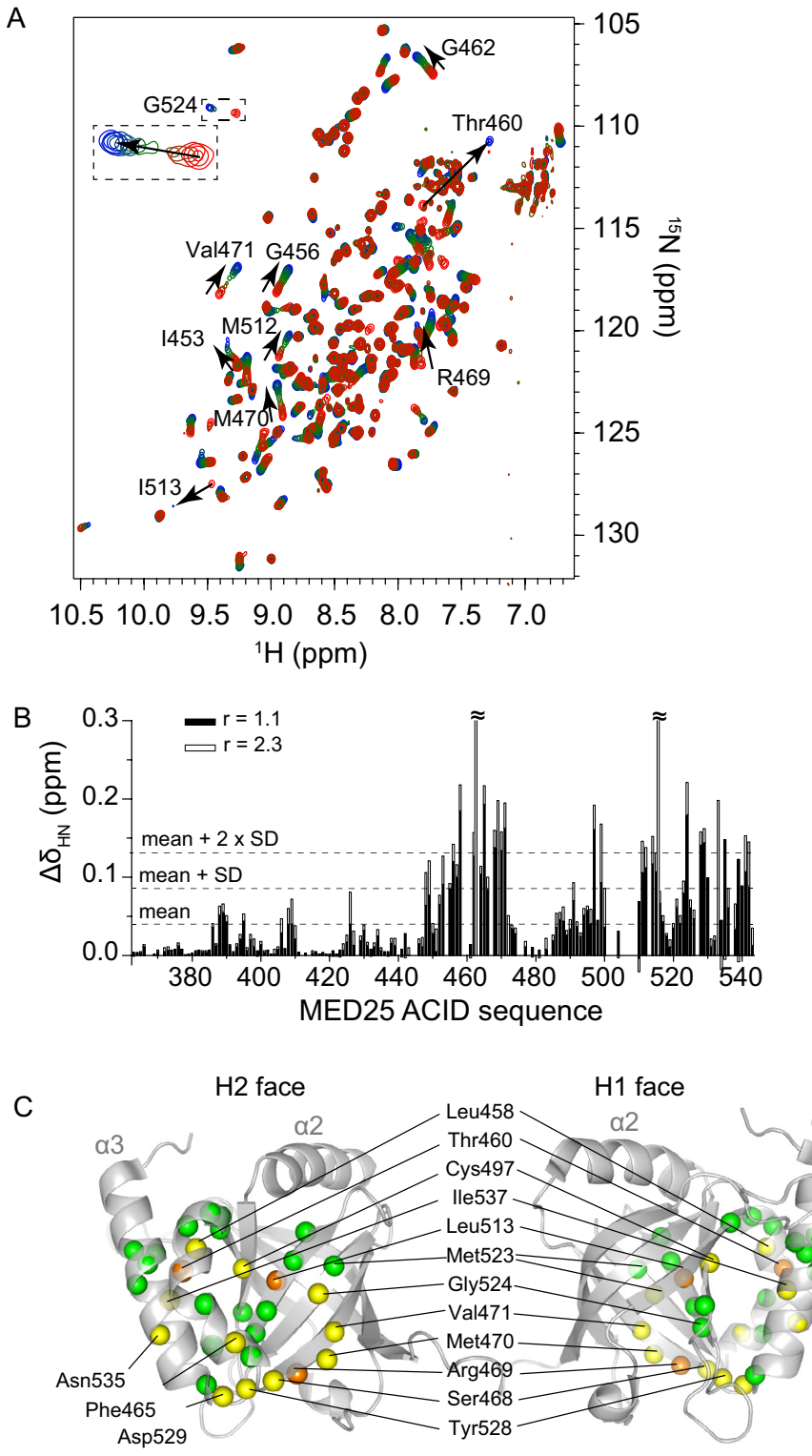
A
G462
G524
Thr460
Val471
G456
I453
M512
R469
M470
I513
105
110
115
120
125
130
^{15}N (ppm)
10.5 10.0 9.5 9.0 8.5 8.0 7.5 7.0
^{1}H (ppm)
B
r = 1.1
r = 2.3
mean + 2 x SD
mean + SD
mean
0.3
0.2
0.1
0.0
$\Delta\delta_{HN}$ (ppm)
380 400 420 440 460 480 500 520 540
MED25 ACID sequence
C
H2 face
H1 face
α3
α2
α2
α3
Leu458
Thr460
Cys497
Ile537
Leu513
Met523
Gly524
Val471
Met470
Arg469
Ser468
Tyr528
Asn535
Phe465
Asp529

significant CSPs. CSPs for residues with linear trajectories and a titration endpoint at r = 1.7–2.3, exemplified by Leu452, Met470 and Met512 (Figure 5(A)), were well fitted with a single binding site model (Figure 5(B)). An average value of 17 ± 8 μM was calculated from 48 ^{1}H and ^{15}N titration curves with chemical shift differences between free and bound forms satisfying $\Delta\delta H > 0.08$ ppm or $\Delta\delta N > 0.8$ ppm. The NMR-derived affinity is in line with the value obtained by ITC. The affinity of the NS1α3 peptide for MED25 ACID is slightly lower, but still of the same order of magnitude, than those reported for other single domain TADs, when using peptides in interaction experiments: 0.5 μM for ATF6α, 8 μM for p53TAD2, μM range for VP16-TAD2.[29,33,34]

The resonance frequency difference between free and NS1α3-bound MED25 ACID forms in the intermediate exchange can be used to estimate an exchange rate between free and bound MED25 ACID: we determined a k_{ex} of ∼500 s^{-1}. k_{ex} is a combination of association (k_{on}) and dissociation (k_{off}) rates: $k_{ex} = k_{off} + k_{on} \times$ [MED25 ACID]. Under similar concentration conditions (225 μM MED25 ACID), k_{ex} for VP16 tandem TAD, ERM and ATF6α single domain TADs would be 2–3 orders of magnitudes higher, based on values reported in 33: k_{on} (300–1100 $\mu M^{-1}s^{-1}$) and k_{off} (102–380 s^{-1}). This difference is mainly due to fast association kinetics.[33] K_D values for these 3 TADs were reported to be rather low in the 60–590 nM range.[33] At this point we cannot separate the contributions of dissociation and association in k_{ex}, but taken together, our results suggest that the relatively high K_D value for the NS1α3-MED25 ACID complex is correlated to slow kinetics. Folding of the NS1α3 peptide, which is unstructured in its free form as shown above, upon binding would explain a slower association process.

On closer inspection, it appears that saturation was not achieved at r = 2.3 for all residues, as exemplified by Leu448 in Figure 5(A). In contrast to residues for which saturation is reached at r = 2.3 and which bind to the H2 face of MED25 ACID (red spheres in Figure 5(C)), these residues cluster on the H1 face (blue spheres in Figure 5 (C)). The H1 face is the binding site for the TAD1 domain of VP16 (29, 30). A third set of residues, like Ile453 and Ile541, displayed nonlinear CSP trajectories with a change at $r \sim 1.7$, indicating sequential binding events (Figure 5(A)). These residues are mainly located in the junction between the H1 and H2 faces or on the H1 face (purple spheres in Figure 5(C)). As the direction change of CSP trajectories occurs at a molar ratio of 1.7, at which saturation is nearly complete for the H2 binding site, the second binding site H1 must be of lower affinity. Apparent K_d values were extracted from the binding curves of residues on the H1 face and on the H1-H2 interface. These values were in the 200 μM–1 mM range, and higher by 2–3 orders of magnitude than the H2 site K_ds (Figure 5(B)), pointing to a second binding site of lower affinity on the H1 face. The overall behaviour of NS1α3 is reminiscent of VP16 TAD2 that binds to the H2 face *in vitro*, but is also able to bind to H1 with lower affinity.[32]

In order to validate the binding site of highest affinity, i.e. the H2 site, we generated three MED25 ACID single amino acid and one double mutant constructs, all located on the H2 binding face. Specifically, MED25 ACID S468A, M470A, M523E and M470A/M523E mutants were analysed for interaction with NS1. The location of these mutants is shown in Figure 5(D), right panel. We co-expressed recombinant GST-NS1 with WT or mutant MED25 ACID protein in *E. coli* and used GST-pulldown assay (Figure 5(D), left panel). Bacteria lysates were incubated with glutathione beads, washed extensively and the bound complexes were analysed by SDS-PAGE and Coomassie blue staining. All MED25 ACID mutant proteins were expressed to similar levels to WT (data not shown). As shown in Figure 5(D), MED25 ACID was pulled down by GST-NS1 in agreement with the results shown in Figure 3(A).

Figure 4. Interaction of the NS1α3 peptide with MED25 ACID followed by NMR. (A) Overlay of 2D ^{1}H-^{15}N HSQC spectra acquired during a titration of 225 μM ^{15}N-labeled MED25 ACID with increasing amounts of NS1α3 peptide. The reference spectrum without peptide is shown in red. The last titration point with a peptide:protein molar ratio r = 2.3 is in medium blue. Intermediate titration points at r = 0.1, 0.2, 0.4, 0.6, 0.85, 1.1, 1.4, and 1.7 are colour coded from dark orange to dark blue. Arrows show the titration direction for several noticeable signals. The inset shows a close-up of the titration curve for the Gly524 residue. **(B)** Combined ^{1}H and ^{15}N amide chemical shift perturbations (CSPs) $\Delta\delta_{HN}$ are represented as bar diagrams as a function of the residue number in the MED25 ACID construct at titration points r = 1.1 (black bars) and r = 2.3 (empty bars). The bars at r = 2.3 were cut for residues Thr460 and Leu513 ($\Delta\delta_{HN} > 0.3$ ppm). Broken lines indicate the mean value and mean plus one and two standard deviations (SD) for r = 1.1. **(C)** Chemical shift perturbations of residues in a fast or fast-to-intermediate exchange regime at r = 1.1 were mapped onto the structure of MED25 ACID (pdb 2xnf). Amide nitrogen atoms are drawn as yellow spheres for residues with combined ^{1}H and ^{15}N CSPs $\Delta\delta_{HN} \geq$ mean + 2 × SD and as green spheres for residues with $\Delta\delta_{HN} \geq$ mean + SD. Amide nitrogen atoms of residues in an intermediate exchange regime are drawn as orange spheres. The two views correspond to the H2 and H1 faces of MED25 ACID, and are rotated by ∼180°.

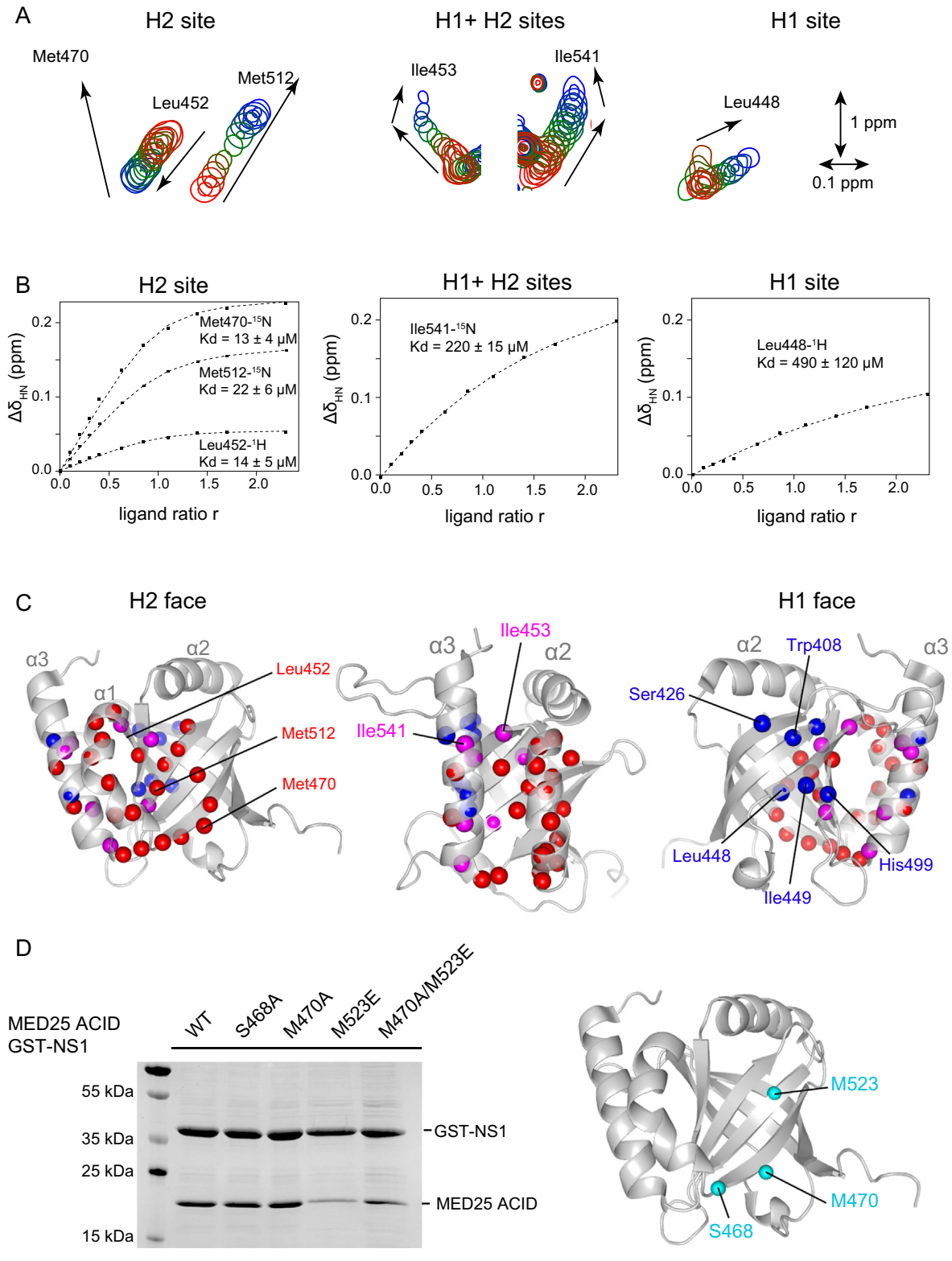
A
H2 site
H1+ H2 sites
H1 site
Met470
Leu452
Met512
Ile453
Ile541
Leu448
1 ppm
0.1 ppm
B
H2 site
H1+ H2 sites
H1 site
Met470-15N
Kd = 13 ± 4 μM
Met512-15N
Kd = 22 ± 6 μM
Leu452-1H
Kd = 14 ± 5 μM
Ile541-15N
Kd = 220 ± 15 μM
Leu448-1H
Kd = 490 ± 120 μM
Δδ HN (ppm)
ligand ratio r
C
H2 face
H1 face
α1
α2
α3
Leu452
Met512
Met470
Ile453
Ile541
Trp408
Ser426
Leu448
His499
Ile449
D
MED25 ACID
GST-NS1
WT
S468A
M470A
M523E
M470A/M523E
55 kDa
35 kDa
25 kDa
15 kDa
GST-NS1
MED25 ACID
M523
M470
S468

MED25 ACID S468A and M470A showed similar binding to NS1. In contrast, binding of MED25 ACID M523E to NS1 was strongly reduced. The MED25 ACID M470A/M523E double mutant also showed reduced affinity (Figure 5(D)), confirming the role of the M523 residue in NS1 binding.

In conclusion, we showed by NMR that the NS1α3 peptide preferentially binds to the MED25 ACID H2 face with an affinity in the 10–20 μM range, corroborating our ITC measurements. This low affinity may be explained by the lack of α-helical structure in the NS1α3 peptide as compared to NS1 protein. Mutational analysis of MED25 ACID confirmed that NS1 targets the H2 face of MED25 ACID.

NS1 competes with ATF6α for binding to MED25 ACID

MED25 is a target of several transcriptional activators, from cellular and viral origin,[29–32,34,46] which bind either to the H1 or H2 faces of MED25 ACID through their TAD domains.[33] Previous studies have shown that the endoplasmic reticulum stress-responsive transcription factor α (ATF6α), that functions as a master regulator of ER stress response, also targets MED25,[47,48] and that the TAD of ATF6α (residues 40–66, Figure 6(A)) binds to the H2 site.[33] Since our NMR results indicated that NS1 α3 helix binds to H2, we wondered whether NS1 could compete with a TAD domain, by using ATF6α. A GST-ATF6α construct containing the TAD domain (GST-ATF6α TAD, residues 1–150), bound to glutathione beads, was incubated with recombinant MED25 ACID (30 μM) without or with 15 and 30 μM of NS1 protein. The bound fractions were then analysed by SDS-PAGE and Coomassie blue staining. GST alone was used as a negative control. Purified proteins are shown in Figure 6(B). MED25 ACID was pulled down by GST-ATF6α TAD, but not by GST (Figure 6(C)), as previously published.[47,48] Adding NS1 inhibited MED25 ACID binding to GST-ATF6α TAD (Figure 6(C)). These data suggest that NS1 is able to compete for MED25 ACID binding with an H2-binding TAD domain such as ATF6αTAD.

Discussion

NS1 interacts with MED25

A previous proteomics study aiming to identify host partners of RSV NS1 identified several proteins involved in transcription regulation, among them Mediator complex proteins.[22] Recent NS1 co-immunoprecipitation and mass spectrometry analysis also identified subunits of the complex, among them MED25.[18] By using a Y2H screen, we identified MED25 as an interacting partner of NS1. Our NanoLuc interaction assay confirmed the NS1-MED25 interaction in cells and identified MED25 ACID and the NS1 C-terminal α3 helix of NS1 as interaction domains (Figure 2). Our GST pull-down experiment (Figure 3(A)) and ITC results (Figure 3(B)) showed that the NS1/MED25 ACID interaction is direct and of high affinity (20 nM). We were able to confirm direct binding of the NS1 α3 helix to MED25 ACID *in vitro*, but our GST pull-down experiments suggest that the NS1 α,β-core domain can also contribute to MED25 ACID binding.

The NS1 α3 helix was previously shown to contribute to the modulation of host response to RSV infection.[18,20] Mutation of residues Y125, and L132/L133 in the NS1 α3 helix or truncation of the entire α3 helix impacted the ability of NS1 to inhibit type I IFN. Moreover, recombinant RSV viruses carrying these mutations showed attenuated

Figure 5. The NS1α3 peptide binds to MED25 ACID H1 and H2 faces with different apparent affinities. (A) Five chemical shift perturbation trajectories corresponding to fast or fast-to-intermediate exchange regimes were extracted from ^{1}H-^{15}N HSQC spectra measured during titration of of ^{15}N-MED25 ACID by the NS1α3 peptide. Arrows show the titration direction. The colour is varied from red to medium blue for molar peptide:protein ratios $r = 0$ to 2.3, with titration points at $r = 0.1$, 0.2, 0.3, 0.4, 0.6, 0.85, 1.1, 1.4, and 1.7. They are shown at the same chemical shift scale (given on the right side) and exemplify different behaviors with different titration endpoints or a change in the titration trajectory. **(B)** ^{15}N and ^{1}H chemical CSPs extracted from the trajectories shown in A were fitted with a single binding site model, assuming fast chemical exchange. Experimental points are represented with solid symbols and the fitted curve in broken lines. The apparent dissociation constant K_d and the fitting error are indicated above or below the curve. **(C)** Residues with large ^{1}H and/or ^{15}N CSPs, i.e. with chemical shift differences between free and bound forms of $\Delta\delta H > 0.08$ ppm and/or $\Delta\delta N > 0.8$ ppm, and for which K_d values were measured in the 7–40 μM range, were mapped onto the structure of MED25 ACID (pdb 2xnf): their amide nitrogens are represented as red spheres. Residues with linear CSPs, for which saturation was not achieved at $r = 2.3$, displaying CSP amplitudes $\Delta\delta H > 0.04$ ppm and/or $\Delta\delta N > 0.4$ ppm at $r = 2.3$, are shown in blue. Residues that display a change in CSP trajectory are represented in magenta. The three views are rotated by 90°. **(D)** GST-NS1 was co-expressed together with MED25 ACID WT or mutant protein in *E. coli* BL21(DE3) bacteria. Bacteria lysates were clarified and the soluble protein complexes were purified on glutathione-Sepharose beads. After extensive washing the binding of MED25 ACID to GST-NS1 was analysed by SDS-PAGE and Coomassie blue staining. The position of mutated residues is indicated by cyan spheres on the structure of MED25 ACID on the right side.

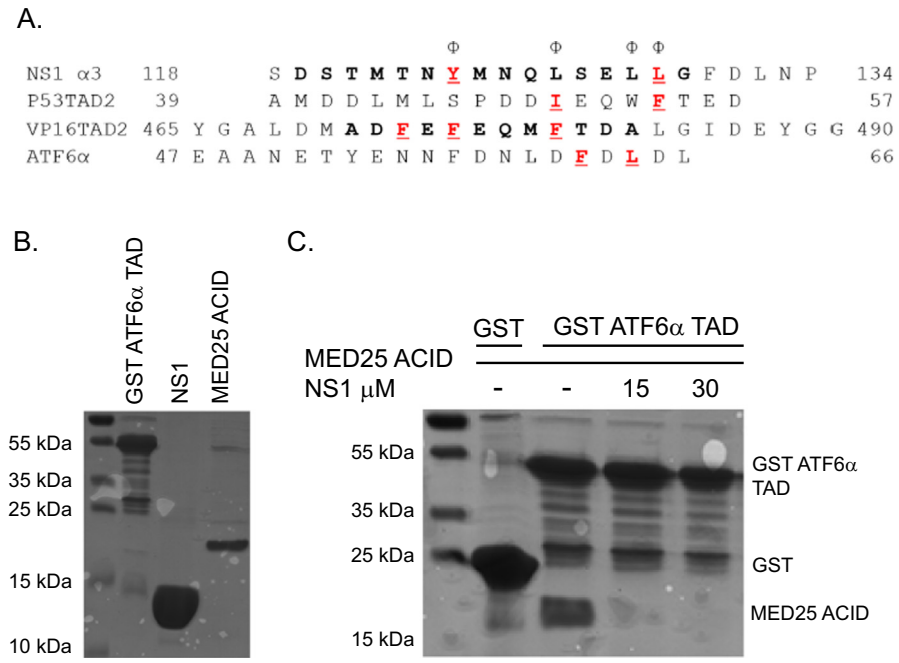

Figure 6. NS1 competes with ATF6α for binding to MED25. (A) Sequence alignment of NS1 α3 with transactivator domains of transcription factors VP16, p53 and ATF6α that bind to the H2 face of MED25 ACID.[20,29,34,48] The letter Φ indicates hydrophobic or aromatic amino acids. Bold letters indicate residues that were reported to fold into an α-helix: for VP16 TAD2 bound to MED25 ACID,[29] and for NS1 α3 in the context of the unbound full-length protein.[20] Underlined red letters indicate residues that are critical for the interaction of NS1 α3, p53TAD2 and ATF6α with MED25 ACID or critical for transcription in yeast for VP16TAD2. **(B)** SDS-PAGE and Coomassie blue staining of purified recombinant GST-ATF6α TAD, NS1 and MED25 ACID protein. **(C)** GST or GST-ATF6α TAD were expressed in *E. coli* BL21(DE3), purified on glutathione-Sepharose beads, and incubated in the presence of 30 μM MED25 ACID without or with 15 and 30 μM NS1, as indicated. After extensive washing the binding of MED25 ACID to GST and GST-ATF6αTAD was determined by SDS-PAGE and Coomassie blue staining.

replication in IFN-competent cells and differential gene expression in the IFN pathways as compared to WT RSV.[20] We show here that two of these amino acids (Y125 and L133) are also critical for MED25 ACID interaction. Importantly these NS1 α3 helix point mutants can still properly localize to the nucleus (Figure 2(E)), indicating that these mutations do not impair NS1 nuclear localization and are accessible to MED25. Strikingly, in the dimeric crystal structure of NS1, L132 and Y125 make intra-protomer and inter-protomer contacts, suggesting that they are buried in the structure and not available for interactions. L133 makes only inter-protomer contacts. If NS1 is monomeric, Y125 and L132 become accessible, whereas L133 anchors the α3 helix to the α,β-core of NS1. Since L133 appears to be critical for targeting MED25, this raises the question whether the α3 helix may dissociate from the α,β-core for MED25 binding.

We further confirmed by NMR that the NS1α3 peptide (Figures 4 and 5) directly interacts with MED25 ACID and preferentially binds to the H2 face of MED25 ACID, like several TADs of transcriptional regulators.[29,32–34] Binding of NS1 to the H2 face was validated by GST-pulldown assays, where the MED25 ACID M523E mutation impaired binding to GST-NS1 (Figure 5(D)). The K_d of 10 μM obtained by ITC and the mean K_d of 17 μM obtained by NMR for NS1α3 peptide binding to the H2 face indicate rather weak affinity and may question the relevance of NS1 α3 binding to MED25 ACID. We showed that the NS1α3 peptide, used to perform interaction experiments, lacked α-helical conformation in its free form, contrary to the NS1 α3 helix that is preformed in the NS1 protein. The low affinity may therefore be linked to the additional folding process. However, since we observed that the α,β-core domain of NS1 can also bind MED25 ACID, this domain may complement NS1 α3 binding.

Our ^{1}H-^{15}N HSQC NMR titration experiment display similar features to those reported for canonical TADs, i.e. a fast chemical exchange regime for many perturbed signals, line broadening for residues with large chemical shift amplitudes and similar concentrations to reach saturation, suggesting similar binding modes and affinities.[29,33,34] The affinity of MED25 ACID for the VP16 tandem TAD was estimated to be low μM to high nM by NMR,[29] and later a K_d of 60 nM

was measured by fluorescence anisotropy.[33] Higher affinities were also measured for ATF6α TAD (0.5 μM) by fluorescence anisotropy[33] and for the p53 tandem TAD (0.8 μM) by ITC.[34] In contrast, for VP16 TAD2, which binds to the H2 face, an 8-fold molar excess of peptide was needed to reach saturation in an NMR titration experiment, which is indicative of μM affinity,[29] and p53TAD2 was shown to bind with 8 μM affinity.[34] This suggests that the results obtained with NS1α3 are comparable to those obtained with other TADs under similar experimental conditions.

Comparing the sequences of the three H2-binding TADs (VP16, p53 and ATF6α) with that of NS1 α3 did not reveal any striking sequence similarity (Figure 6(A)). Even residues that are critical for binding to MED25 ACID or important for MED25 function do not display any common pattern, apart from the requirement for hydrophobic residues (Figure 6(A)). This is rather intriguing, but might underline that binding occurs through a multi-step process, with specificities for each TAD, as already pointed out by Henderson et al.[33] The low exchange rate measured by NMR for NS1α3 binding would be specific of NS1.

NS1 competes with cellular TADs for targeting MED25

Transcription activator ATF6α functions as a master regulator of ER stress response. In response to ER stress, ATF6α translocates to the Golgi, where it is processed, followed by transport to the nucleus, where it activates the unfolded protein response (UPR) genes.[49,50] ATF6α was shown to recruit the Mediator complex by binding directly to the MED25 subunit,[48] via the H2 site on MED25 ACID.[33] Our NMR analysis showed binding of NS1 to the MED25 ACID H2 site (Figures 4 and 5), suggesting that NS1 might be able to compete for MED25 with ATF6α. Moreover, the same MED25 ACID mutant M523E results in significant loss of binding for both NS1 and ATF6α, with a 9-fold increase of the dissociation constant reported for ATF6α.[33] Our competition studies showed an absence of MED25 ACID binding to ATF6α in the presence of NS1 (Figure 6(C)), favouring this hypothesis.

Very recently it was shown that the cellular UPR response is central to adaptation of glycoprotein metabolism in RSV.[51] RSV infection activates the UPR, partly by inducing a spliced form of X-box binding protein 1 (XBP1) and partly by processing and activating ATF6α, both proteins being central arms of the UPR response. This was suggested to enhance virus production and to have a positive effect on virus-induced structural airway remodelling.[51] While our study suggests that RSV could de-activate ATF6α through competition by NS1 for MED25 binding, it is possible that activating and de-activating ATF6α needs to be carefully balanced during RSV infection. Even as viruses utilize the host UPR to enhance virus production and host cell survival, the invoked UPR in turn has the potential to sense viral infection and trigger anti-viral responses.[52]

Furthermore, NS1 was shown to associate with chromatin, and gene regulatory elements such as enhancers of genes differentially expressed during RSV infection were singled out, suggesting a new role for NS1 in regulating host gene transcription.[18] Importantly, 43% of NS1 peaks identified by Chip-seq analysis coincided with Mediator peaks.[18] Our results show a direct interaction between NS1 and MED25 via the H2 face of MED25 ACID, which rationalizes NS1 association with Mediator peaks.[18] Moreover, the Chip-seq analysis showed that the NS1 α3 helix mutant Y125A did not impact NS1 binding to chromatin, but modulated gene expression, which suggested that the α3 helix may be important for interaction with a cellular partner, such as MED25, regulating host transcription.[18]

MED25 has recently emerged as one of the most significant targets for functional interactions with a range of transcriptional activators, including Herpes simplex virus transactivation protein VP16,[30,32] ATF6α,[48] ERM transcription factor,[31] and p53.[34] Cellular and viral transcriptional activators that target MED25 are multi-domain proteins, which contain at least one transactivation domain (TAD) that binds the transactivator Mediator subunit MED25 and a DNA-binding domain that recognizes specific promoters/signals on target genes, which are then transcribed by RNA Pol II. Our results suggest that NS1 possesses a TAD domain. No specific DNA-binding region has been identified for NS1 yet. We therefore hypothesize that this TAD contributes to displace those of other regulation factors from the Mediator complex, thereby reducing related activation. Moreover, RSV NS1 and NS2 are the most abundantly transcribed RSV genes.[17] On this basis we propose that NS1 could act as a transcription suppressor. This would present a new mechanism to control the host response upon RSV infection by interfering with activation of innate immune response genes by cellular transcriptional activators.

Materials and Methods

Plasmid constructs

Custom synthesized pciNanoLuc 114 and 11S vectors (GeneCust) were used to clone the codon-optimized hRSV NS1 and MED25 constructs using standard PCR, digestion and ligation techniques. pcineo NS1 single site mutants in the full-length construct as well as insertion of the FLAG tag into NS1 and MED25 constructs were generated by using the Q5 site-directed mutagenesis kit (New England BioLabs), following the manufacturer recommendations. pGEX4T3 was used to clone NS1 using standard PCR, digestion and ligation

techniques. pGEX NS1 α3, and pGEX NS1 Δα3 constructs were re-cloned from pcineo NS1 vector using standard PCR, digestion and ligation techniques. MED25 (Addgene) deletion mutants were obtained by introducing start and stop codons at the appropriate site in the coding sequence (MED25 VWD aa 1–231 and MED25 ACID aa 389–543). MED25 ACID was cloned into pET28-derived plasmid using standard PCR, digestion and ligation techniques. MED25 ACID mutants were generated by quick change mutagenesis. pet41s GST ATF6αTAD (aa 1–150) (Addgene) contained the TAD domain.

Y2H screen

The Y2H screen was performed as previously described.[35] The DNA sequence encoding RSV NS1 was cloned by *in vitro* recombination (Gateway technology; Invitrogen) from pDONR207 into the Y2H vector pPC97-GW to be expressed as a fusion protein with the GAL4 DNA-binding domain (GAL4-BD). AH109 yeast cells (Clontech; Takara, Mountain View, CA, USA) were transformed with this construct using a standard lithium-acetate protocol. Screens were performed on a synthetic medium lacking histidine (-His) and supplemented with 3-amino-1,2,4-triazole (3-AT). A mating strategy was used to screen a commercial human spleen cDNA library (Invitrogen) and a human full-length ORF library (hORFeome)[53] established in the pPC86 vector to express cellular proteins in fusion downstream of the GAL4 transactivation domain (GAL4-AD). After 6 days of culture, colonies were picked and replica plated over three weeks to maintain selection and eliminate potential contaminants. cDNA inserts were amplified from positive yeast colonies using primers that hybridize within the backbone of the pPC86 vector. After sequencing of the PCR products, cellular interactors were identified by multi-parallel BLAST analysis.

Bacteria expression and purification of recombinant proteins

MED25 ACID (residues Leu389-Asn543) was produced with an N-terminal 6xHis-tag followed by a T7 tag from a pET28-derived plasmid. *E. coli* BL21(DE3) bacteria transformed with the pET28 MED25 ACID plasmid were grown from fresh starter culture in Luria-Bertani (LB) broth at 37 °C to an optical density of 0.6 at 600 nm, followed by induction with 0.2 mM isopropyl-β-D-thiogalacto side (IPTG) for 18 h at 20 °C. Cells were lysed by sonication (4 times for 20 s each time) and lysozyme (1 mg/ml; Sigma-Aldrich) in 50 mM Na phosphate, 300 mM NaCl, 10 mM imidazole pH 8, plus protease inhibitors (Roche). Lysates were clarified by centrifugation (23,425*g*, 30 min, 4 °C), and the soluble MED25 ACID protein was purified on 1 ml beads loaded with Ni-NTA (GE Healthcare). The bound protein was washed extensively with loading buffer containing 50 mM Na phosphate, 300 mM NaCl and 25 mM imidazole and eluted with 50 mM Na phosphate, 300 mM NaCl and 250 mM imidazole pH 8.

^{15}N- and $^{15}N^{13}C$-labelled MED25 ACID samples were produced in minimal M9 medium supplemented with 2 mM $MgSO_4$, 100 μM $CaCl_2$, 0.5X MEM vitamin solution (Gibco), 30 $\mu g \cdot mL^{-1}$ kanamycin, 1 $g \cdot L^{-1}$ $^{15}NH_4Cl$ (Eurisotop, France) and 4 $g \cdot L^{-1}$ glucose or 3 $g \cdot L^{-1}$ ^{13}C-glucose (Eurisotop, France). Expression was induced with 0.1 mM IPTG. Lysis, clarification and purification, using 2 mL Ni-NTA resin (ThermoFisher, France) per liter of culture, were carried out as described for unlabelled MED25 ACID. The eluted His-tagged protein was then dialyzed into 20 mM Na phosphate pH 6.5, 100 mM NaCl buffer supplemented with 0.5 mM dithiothreitol (DTT) using a 10 kDa cut-off membrane (Spectrapor). The protein samples were further purified by gel filtration on a Superdex S75 HR 10/30 column (GE Healthcare). Samples were then concentrated to ~500 μM using 10 kDa cut-off centrifugal filter units (Amicon Ultra, Millipore), and the DTT concentration was raised to 5 mM. The MED25 ACID concentration was determined by measuring the absorption at 280 nm and applying a molar extinction coefficient of 22,460 $mol^{-1} \cdot cm^{-1}$.

For NS1 expression, *E. coli* BL21(DE3) bacteria transformed with the pGEX-NS1 plasmid were grown from fresh starter culture in LB broth at 37 °C to an optical density of 0.8 at 600 nm, followed by induction with 0.5 mM IPTG for 18 h at 20 °C. Cells were lysed by sonication (4 times for 20 s each time) and lysozyme (1 mg/ml; Sigma) in 20 mM Tris–HCl, 300 mM NaCl, 5% glycerol, pH 8, plus protease inhibitors (Roche). Lysates were clarified by centrifugation (23,425*g*, 30 min, 4 °C), and the soluble GST-NS1 was purified on 1 ml Glutathione Sepharose beads (cytiva). The bound protein was washed with 20 mM Tris–HCl, 1 M NaCl, 5% glycerol, pH 8, followed by wash with 20 mM Tris–HCl, 300 mM NaCl, 5% glycerol, 5 mM 2-mercaptoethanol, pH 8. GST-NS1 beads were then washed with 20 mM Tris–HCl, 150 mM NaCl, 2.5 mM $CaCl_2$, 5 mM 2-mercaptoethanol, pH 8 and incubated with Biotinylated-thrombin protease (Novagen) over night at 4C. The supernatant NS1 fraction was collected and incubated with Streptavidin agarose (Millipore) for 1 h at 4 °C in order to eliminate Thrombin. Purified NS1 was then concentrated using Vivaspin columns (SartoriusStedimBiotec).

For GST and GST-ATF6αTAD expression, *E. coli* BL21(DE3) bacteria transformed with the pGEX or pet41s-ATF6α plasmid were grown from fresh starter culture in LB broth at 37 °C to an optical density of 0.5 at 600 nm, followed by induction with 1 mM IPTG for 18 h at 16 °C. Cells were lysed by sonication (4 times for 20 s each time)

and lysozyme (1 mg/ml; Sigma) in 50 mM Tris–HCl, 300 mM NaCl, pH 8, plus protease inhibitors (Roche). Lysates were clarified by centrifugation (23,425*g*, 30 min, 4 °C), and the soluble GST-ATF6αTAD protein was purified on 1 ml glutathione Sepharose beads (cytiva). The bound protein was washed extensively with 50 mM Tris–HCl and 150 mM NaCl, pH 8. GST-ATG6α was eluted by incubating the glutathione beads with 50 mM reduced glutathione for 1 h at RT. The eluted protein was then dialysed for 18 h into 50 mM Tris–HCl and 150 mM NaCl, pH 8, to eliminate free Glutathione. GST-ATF6α was concentrated to 2 ml using Vivaspin4 column (SartoriusStedimBiotec) and purified on a HiLoad 10/600 Superdex S200 column (GE Healthcare). Clean GST-ATF6α fraction was used directly to rebind to glutathione beads for competition experiments.

Peptide preparation

N-acetylated NS1α3 peptide Ac-SDSTMTNYMNQLSELLGFDLNP (RSV NS1 residues Ser118-Pro139) was synthesized by GeneCust (Luxemburg) with >95% purity, as assessed by HPLC and subsequently by NMR. Aliquots of 2 mg were suspended in 1 mL MQ water and dispersed by sonication. The pH was neutralized by addition of 1 M NaOH, leading to complete dissolution. The concentration was determined by measuring the absorption at 280 nm and applying a molar extinction coefficient of 1490 $mol^{-1} \cdot cm^{-1}$. The quality of the peptide solution was assessed by NMR. The concentration was verified by 1D ^{1}H NMR under quantitative conditions by comparing peptide signal intensities with those of sodium trimethylsilylpropanesulfonate (DSS) added as an internal standard with known concentration. Aliquots were lyophilized for the titration experiment with ^{15}N-MED25 ACID.

Pull-down experiments

MED25 ACID WT or mutant construct was co-expressed together with GST, GST-NS1, GST-NS1 Δα3 or GST-NS1 α3 helix. *E. coli* BL21(DE3) bacteria were transformed with the pet28 MED25 ACID plasmids together with empty pGEX, pGEX NS1, GST-NS1 Δα3, or pGEX NS1 α3 helix. Protein induction was as for MED25 ACID alone (see above). Cells were lysed by sonication (4 times for 20 s each time) and lysozyme (1 mg/ml; Sigma) in 50 mM Na Phosphate, 300 mM NaCl, pH 8, plus protease inhibitors (Roche). Lysates were clarified by centrifugation (23,425*g*, 30 min, 4 °C), and the soluble proteins complexes were purified on 1 ml Glutathione Sepharose beads (cytiva). Beads were washed with 50 mM Tris–HCl and 150 mM NaCl, pH 8, and the bound proteins were analysed by SDS-PAGE and Coomassie staining. For pull-down experiment between GST-NS1 and WT and mutant MED25 ACID constructs in Figure 5(D), beads were washed with 50 mM Tris–HCl and 300 mM NaCl, pH 8.

Cell culture

293T cells were maintained in Dulbecco modified Eagle medium (eurobio) supplemented with 10% fetal calf serum (FCS; eurobio), 1% L-glutamine, and 1% penicillin streptomycin. The transformed human bronchial epithelial cell line (BEAS-2B) (ATCC CRL-9609) was maintained in RPMI 1640 medium (eurobio) supplemented with 10% fetal calf serum (FCS; eurobio), 1% L-glutamine, and 1% penicillin–streptomycin. The cells were grown at 37 °C in 5% CO_2.

NS1-ATF6αTAD competition assay

GST and GST-ATF6αTAD were expressed in BL21 *E. coli* and purified on Glutathione beads as described above. 40 μl GST or GST-ATF6α TAD beads were incubated with 30 μM purified MED25 ACID without or with 15 and 30 μM of NS1 protein for 2 h at 4 °C. After incubation, the supernatants were collected for analysis. Beads were washed with 50 mM Tris–HCl and 150 mM NaCl, pH 8, and the samples corresponding to proteins bound to beads or recovered in the supernatant were analysed by SDS-PAGE and Coomassie blue staining.

NanoLuc interaction assay

Constructs expressing the NanoLuc subunits 114S and 11S were used.[37] 293T cells were seeded at a concentration of 3×10^4 cells per well in 48-well plate. After 24 h, cells were co-transfected in triplicate with 0.4 μg of total DNA (0.2 μg of each plasmid) using Lipofectamine 2000 (Invitrogen). 24 h post transfection cells were washed with PBS, and lysed for 1 h in room temperature using 50 μl NanoLuc lysis buffer (Promega). NanoLuc enzymatic activity was measured using the NanoLuc substrate (Promega). For each pair of plasmids, three normalized luminescence ratios (NLRs) were calculated as follows: the luminescence activity measured in cells transfected with the two plasmids (each viral protein fused to a different NanoLuc subunit) was divided by the sum of the luminescence activities measured in both control samples (each NanoLuc fused viral protein transfected with an plasmid expressing only the NanoLucsubunit). Data represent the mean ± SD of 4 independent experiments, each done in triplicate. Luminescence was measured using Infinite 200 Pro (Tecan, Männedorf, Switzerland).

Immunostaining and imaging

Overnight cultures of BEAS-2B cells seeded at 4 10^5 cells/well in 6-well plates (on a 16-mm micro-

cover glass for immunostaining) were transfected with pcineo plasmids (0.4 μg) carrying the RSV codon-optimised NS1 or FLAG-NS1 WT or mutant constructs using Lipofectamine 2000 (Invitrogen) according to the manufacturer's recommendations. At 24 h post transfection cells were fixed with 4% paraformaldehyde in PBS for 10 min, blocked with 3% BSA in 0.2% Triton X-100–PBS for 10 min, and immunostained with monoclonal anti-FLAG (1:2000; Sigma) antibodies, followed by species-specific secondary antibody conjugated to Alexa Fluor 488 (1: 1,000; Invitrogen). Images were obtained using Nikon TE200 inverted microscope equipped with a Photometrics CoolSNAP ES2 camera. Images were processed using MetaVue software (Molecular Devices).

SDS-PAGE and Western analysis

Protein samples were separated by electrophoresis on 12% or 15% polyacrylamide gels in Tris-glycine buffer. All samples were boiled for 3 min prior to electrophoresis. Proteins were then transferred to a nitrocellulose (for NS1 and P proteins) (Roche) or PVDF (for MED25 proteins) (Roche) membrane. The blots were blocked with 5% non-fat milk in Tris-buffered saline (pH 7.4), followed by incubation with monoclonal anti-FLAG (1:2,000, Sigma), or rabbit anti-P antiserum (1:5,000),[38] and horseradish peroxidase (HRP)-conjugated donkey anti-mouse (1:10,000) or donkey anti-rabbit (1:10,000) antibodies (P.A.R.I.S.). Western blots were developed using freshly prepared chemiluminescent substrate (100 mM TrisHCl, pH 8.8, 1.25 mM luminol, 0.2 mM p-coumaric acid, 0.05% H_2O_2) and exposed using BIO-RAD ChemiDoc™ Touch Imaging System.

Dynamic light scattering

Dynamic light scattering (DLS) measurements were performed on a Zetasizer Nano S instrument (Malvern) with a 173° angle using a volume of 40 μL in disposable 70 μL cuvettes (Brand). Measurements were carried out at 25 °C.

Isothermal titration calorimetry

ITC measurements were carried out on a VP-ITC calorimeter (MicroCal) at a temperature of 298 K. For titration of NS1 by MED25 ACID, both protein samples were dialyzed against the same batch of 20 mM Tris pH 8.0, 200 mM NaCl, 1 mM TCEP buffer. NS1 (20 μM) was placed into the calorimeter cell (V = 1435 μL) and MED25 ACID (300 μM) was injected in 8 μL volumes. For titration of NS1α peptide by MED25 ACID, MED25 ACID was dialyzed against 20 mM Tris pH 8.0, 200 mM NaCl, 1 mM TCEP buffer. Lyophilized NS1α peptide, for which the pH had been adjusted to 8 before, was solubilized in the same batch of buffer. NS1α3 (20 μM) was placed into the calorimeter cell, and MED25 ACID (420 μM) was injected in 8 μL volumes. Data were processed and analyzed with MicroCal Origin software. Baselines and integration were manually adjusted.

Nuclear Magnetic Resonance (NMR) measurements

NMR measurements on NS1α peptide were carried out on a Bruker Neo 700 MHz NMR spectrometer equipped with a cryogenic TXO probe at a temperature of 298 K. The peptide concentration was 790 μM and the sample contained 7.5% ^2H_2O to lock the spectrometer frequency. 1D ^1H NMR spectra and 2D ^1H–^1H DIPSI2 (mixing time 40 ms), ^1H–^1H ROESY (mixing time 200 ms) and ^1H–^1H NOESY (mixing time 300 ms) were acquired. All spectra were acquired with water suppression using excitation sculpting with gradients.

NMR measurements with MED25 ACID were performed on a Bruker Avance III 800 MHz NMR spectrometer equipped with a cryogenic TCI probe. All samples were prepared in 20 mM Na phosphate pH 6.5, 100 mM NaCl, 5 mM DTT buffer supplemented with 7.5% ^2H_2O. The temperature was set to 293 K. BEST-TROSY versions of triple resonance 3D experiments[54] were acquired on $^{13}C^{15}N$-labeled MED25 ACID (460 μM final concentration) for backbone assignment, with a 0.2 ms recycling delay: HNCO, HNCA, HN(CO)CA, CB-optimized HNCACB and HN(CO)CACB. A standard 3D ^{15}N NOESY-HSQC experiment was recorded at 700 MHz on 300 μM ^{15}N-labeled MED25 ACID to confirm chemical shift assignments. ^1H chemical shifts were referenced to DSS. NMR data were processed within TopSpin 4.0 (Bruker Biospin, Wissembourg) and analysed with Ccp Nmr Analysis 2.4 software.[55] The titration experiment of ^{15}N-MED25 ACID (225 μM) by NS1α3 peptide was carried out by recording 2D ^1H-^{15}N HSQC spectra, using a BEST-TROSY sequence. At each titration point, a lyophilized peptide aliquot was added to keep the protein concentration constant at 225 μM, starting at 0.1 and ending at 2.3 molar equivalents. Combined amide ^1H and ^{15}N chemical shift perturbations $\Delta\delta_{HN}$ were calculated with a scaling factor of 1/10 for ^{15}N, corresponding to the ratio of gyromagnetic ratios between ^{15}N and ^1H (Eq. (1)):

$$\Delta\delta_{HN} = \sqrt{((\delta^1H - \delta^1H_{ref})^2 + (\delta^{15}N - \delta^{15}N_{ref})^2/100)} \quad (1)$$

Dissociation constant K_d values were extracted by fitting MED25 ACID ^1H and/or ^{15}N chemical shift perturbations as a function of the ligand ratio, i.e. the peptide:protein molar ratio (r), with a single site binding model and assuming a fast chemical exchange regime (Eq. (2)), using Ccp Nmr Analysis software.

$$(\delta - \delta_{ref}) = \frac{1}{2}(\delta_{sat} - \delta_{ref}) \times \left(\frac{K_d}{[MED25]_{tot}} + 1 + r - \sqrt{\left(\frac{K_d}{[MED25]_{tot}} + 1 + r\right)^2 - 4r}\right) \quad (2)$$

The exchange rate between free and bound states, k_{ex}, was estimated from the resonance frequency difference $\Delta\nu$ for residues in the intermediate exchange according to $k_{ex} = \pi * \Delta\nu$.

Illustrations

Structural representations were prepared with Pymol (Schrodinger, LLC, The PyMOL Molecular Graphics System 1.3). Graphic rendering of sequence alignment was made with Espript3.0.[56]

CRediT authorship contribution statement

Jiawei Dong: Investigation, Visualization. **Vincent Basse:** Investigation, Visualization. **Maxime Bierre:** Investigation, Visualization. **Andressa Peres de Oliveira:** Investigation. **Pierre-Olivier Vidalain:** Data curation, Investigation. **Pierre Sibille:** Investigation. **Frederic Tangy:** Data curation. **Marie Galloux:** Conceptualization, Writing – original draft. **Jean-Francois Eleouet:** Conceptualization, Supervision, Funding acquisition. **Christina Sizun:** Conceptualization, Supervision, Investigation, Visualization, Writing – original draft, Writing – review & editing, Funding acquisition. **Monika Bajorek:** Conceptualization, Supervision, Investigation, Visualization, Writing – original draft, Writing – review & editing, Funding acquisition.

Acknowledgements

This work was supported by Region Ile de France (DIM 1-HEALTH 2021) and Université Paris Saclay (J.D., doctoral fellowship).

Declaration of interests

The authors declare that they have no known competing financial interests or personal relationships that could have appeared to influence the work reported in this paper.

Appendix A. Supplementary material

Supplementary material to this article can be found online at https://doi.org/10.1016/j.jmb.2022.167763.

Received 23 December 2021;
Accepted 21 July 2022;
Available online 28 July 2022

Keywords:
RSV;
virus-host interaction;
transcription regulation;
mediator;
NMR;
NS1

† Co-first authors.

References

1. Group TPERfCHPS, (2019). Causes of severe pneumonia requiring hospital admission in children without HIV infection from Africa and Asia: the PERCH multi-country case-control study. *Lancet* **394**, 757–779.
2. Shi, T., McAllister, D.A., O'Brien, K.L., Simoes, E.A.F., Madhi, S.A., Gessner, B.D., Polack, F.P., Balsells, E., et al., (2017). Global, regional, and national disease burden estimates of acute lower respiratory infections due to respiratory syncytial virus in young children in 2015: a systematic review and modelling study. *Lancet* **390**, 946–958.
3. Troeger, C., Blacker, B., Khalil, I.A., Rao, P.C., Cao, J., Zimsen, S.R.M., Albertson, S.B., Deshpande, A., et al., (2018). Estimates of the global, regional, and national morbidity, mortality, and aetiologies of lower respiratory infections in 195 countries, 1990–2016: a systematic analysis for the Global Burden of Disease Study 2016. *Lancet Infect. Dis.* **18**, 1191–1210.
4. Coultas, J.A., Smyth, R., Openshaw, P.J., (2019). Respiratory syncytial virus (RSV): a scourge from infancy to old age. *Thorax* **74**, 986–993.
5. Easton, A.J., Domachowske, J.B., Rosenberg, H.F., (2004). Animal pneumoviruses: molecular genetics and pathogenesis. *Clin. Microbiol. Rev.* **17**, 390–412.
6. Valarcher, J.F., Taylor, G., (2007). Bovine respiratory syncytial virus infection. *Vet. Res.* **38**, 153–180.
7. Openshaw, P.J.M., Chiu, C., Culley, F.J., Johansson, C., (2017). Protective and Harmful Immunity to RSV Infection. *Annu. Rev. Immunol.* **35**, 501–532.
8. Russell, C.D., Unger, S.A., Walton, M., Schwarze, J., (2017). The Human Immune Response to Respiratory Syncytial Virus Infection. *Clin. Microbiol. Rev.* **30**, 481–502.
9. Hijano, D.R., Vu, L.D., Kauvar, L.M., Tripp, R.A., Polack, F. P., Cormier, S.A., (2019). Role of Type I Interferon (IFN) in the Respiratory Syncytial Virus (RSV) Immune Response and Disease Severity. *Front. Immunol.* **10**, 566.
10. Bossert, B., Conzelmann, K.K., (2002). Respiratory syncytial virus (RSV) nonstructural (NS) proteins as host range determinants: a chimeric bovine RSV with NS genes from human RSV is attenuated in interferon-competent bovine cells. *J. Virol.* **76**, 4287–4293.
11. Collins, P.L., Karron, R.A., (2013). Respiratory syncytial virus and metapneumovirus. In: Wolters, K. (Ed.), *Chapter in Fields of Virology*. 6th ed., vol. 1..
12. Thornhill, E.M., Verhoeven, D., (2020). Respiratory Syncytial Virus's Non-structural Proteins: Masters of Interference. *Front. Cell. Infect. Microbiol.* **10**, 225.
13. Sedeyn, K., Schepens, B., Saelens, X., (2019). Respiratory syncytial virus nonstructural proteins 1 and 2: Exceptional

disrupters of innate immune responses. *PLoS Pathog.* **15**, e1007984.
14. Van Royen, T., Rossey, I., Sedeyn, K., Schepens, B., Saelens, X., (2022). How RSV Proteins Join Forces to Overcome the Host Innate Immune Response. *Viruses* **14**
15. Boyapalle, S., Wong, T., Garay, J., Teng, M., San Juan-Vergara, H., Mohapatra, S., (2012). Respiratory syncytial virus NS1 protein colocalizes with mitochondrial antiviral signaling protein MAVS following infection. *PLoS ONE* **7**, e29386.
16. Ban, J., Lee, N.R., Lee, N.J., Lee, J.K., Quan, F.S., Inn, K. S., (2018). Human Respiratory Syncytial Virus NS 1 Targets TRIM25 to Suppress RIG-I Ubiquitination and Subsequent RIG-I-Mediated Antiviral Signaling. *Viruses* **10**
17. Swedan, S., Andrews, J., Majumdar, T., Musiyenko, A., Barik, S., (2011). Multiple functional domains and complexes of the two nonstructural proteins of human respiratory syncytial virus contribute to interferon suppression and cellular location. *J. Virol.*. https://doi.org/10.1128/JVI.00413-11.
18. Pei, J., Beri, N.R., Zou, A.J., Hubel, P., Dorando, H.K., Bergant, V., Andrews, R.D., Pan, J., et al., (2021). Nuclear-localized human respiratory syncytial virus NS1 protein modulates host gene transcription. *Cell Rep.* **37**, 109803.
19. Money, V.A., McPhee, H.K., Mosely, J.A., Sanderson, J. M., Yeo, R.P., (2009). Surface features of a Mononegavirales matrix protein indicate sites of membrane interaction. *Proc. Natl. Acad. Sci. U. S. A.* **106**, 4441–4446.
20. Chatterjee, S., Luthra, P., Esaulova, E., Agapov, E., Yen, B.C., Borek, D.M., Edwards, M.R., Mittal, A., et al., (2017). Structural basis for human respiratory syncytial virus NS1-mediated modulation of host responses. *Nature Microbiol.* **2**, 17101.
21. Forster, A., Maertens, G.N., Farrell, P.J., Bajorek, M., (2015). Dimerization of matrix protein is required for budding of respiratory syncytial virus. *J. Virol.* **89**, 4624–4635.
22. Wu, W., Tran, K.C., Teng, M.N., Heesom, K.J., Matthews, D.A., Barr, J.N., Hiscox, J.A., (2012). The interactome of the human respiratory syncytial virus NS1 protein highlights multiple effects on host cell biology. *J. Virol.* **86**, 7777–7789.
23. Flanagan, P.M., Kelleher 3rd, R.J., Sayre, M.H., Tschochner, H., Kornberg, R.D., (1991). A mediator required for activation of RNA polymerase II transcription in vitro. *Nature* **350**, 436–438.
24. Kim, Y.J., Bjorklund, S., Li, Y., Sayre, M.H., Kornberg, R. D., (1994). A multiprotein mediator of transcriptional activation and its interaction with the C-terminal repeat domain of RNA polymerase II. *Cell* **77**, 599–608.
25. Soutourina, J., (2018). Transcription regulation by the Mediator complex. *Nature Rev. Mol. Cell Biol.* **19**, 262–274.
26. Mittler, G., Stuhler, T., Santolin, L., Uhlmann, T., Kremmer, E., Lottspeich, F., Berti, L., Meisterernst, M., (2003). A novel docking site on Mediator is critical for activation by VP16 in mammalian cells. *EMBO J.* **22**, 6494–6504.
27. Yang, F., DeBeaumont, R., Zhou, S., Naar, A.M., (2004). The activator-recruited cofactor/Mediator coactivator subunit ARC92 is a functionally important target of the VP16 transcriptional activator. *Proc. Natl. Acad. Sci. U. S. A.* **101**, 2339–2344.
28. Zhao, H., Young, N., Kalchschmidt, J., Lieberman, J., El Khattabi, L., Casellas, R., Asturias, F.J., (2021). Structure of mammalian Mediator complex reveals Tail module architecture and interaction with a conserved core. *Nature Commun.* **12**, 1355.
29. Vojnic, E., Mourao, A., Seizl, M., Simon, B., Wenzeck, L., Lariviere, L., Baumli, S., Baumgart, K., et al., (2011). Structure and VP16 binding of the Mediator Med25 activator interaction domain. *Nature Struct. Mol. Biol.* **18**, 404–409.
30. Milbradt, A.G., Kulkarni, M., Yi, T., Takeuchi, K., Sun, Z.Y., Luna, R.E., Selenko, P., Naar, A.M., et al., (2011). Structure of the VP16 transactivator target in the Mediator. *Nature Struct. Mol. Biol.* **18**, 410–415.
31. Landrieu, I., Verger, A., Baert, J.L., Rucktooa, P., Cantrelle, F.X., Dewitte, F., Ferreira, E., Lens, Z., et al., (2015). Characterization of ERM transactivation domain binding to the ACID/PTOV domain of the Mediator subunit MED25. *Nucleic Acids Res.* **43**, 7110–7121.
32. Bontems, F., Verger, A., Dewitte, F., Lens, Z., Baert, J.L., Ferreira, E., de Launoit, Y., Sizun, C., et al., (2011). NMR structure of the human Mediator MED25 ACID domain. *J. Struct. Biol.* **174**, 245–251.
33. Henderson, A.R., Henley, M.J., Foster, N.J., Peiffer, A.L., Beyersdorf, M.S., Stanford, K.D., Sturlis, S.M., Linhares, B. M., et al., (2018). Conservation of coactivator engagement mechanism enables small-molecule allosteric modulators. *Proc. Natl. Acad. Sci. U. S. A.* **115**, 8960–8965.
34. Lee, M.S., Lim, K., Lee, M.K., Chi, S.W., (2018). Structural Basis for the Interaction between p53 Transactivation Domain and the Mediator Subunit MED25. *Molecules* **23**
35. Vidalain, P.O., Jacob, Y., Hagemeijer, M.C., Jones, L.M., Neveu, G., Roussarie, J.P., Rottier, P.J., Tangy, F., et al., (2015). A field-proven yeast two-hybrid protocol used to identify coronavirus-host protein-protein interactions. *Methods Mol. Biol.* **1282**, 213–229.
36. Li, S., Armstrong, C.M., Bertin, N., Ge, H., Milstein, S., Boxem, M., Vidalain, P.O., Han, J.D., et al., (2004). A map of the interactome network of the metazoan C. elegans. *Science* **303**, 540–543.
37. Dixon, A.S., Schwinn, M.K., Hall, M.P., Zimmerman, K., Otto, P., Lubben, T.H., Butler, B.L., Binkowski, B.F., et al., (2016). NanoLuc Complementation Reporter Optimized for Accurate Measurement of Protein Interactions in Cells. *ACS Chem. Biol.* **11**, 400–408.
38. Castagne, N., Barbier, A., Bernard, J., Rezaei, H., Huet, J. C., Henry, C., Da Costa, B., Eleouet, J.F., (2004). Biochemical characterization of the respiratory syncytial virus P-P and P-N protein complexes and localization of the P protein oligomerization domain. *J. Gen. Virol.* **85**, 1643–1653.
39. Llorente, M.T., Taylor, I.A., Lopez-Vinas, E., Gomez-Puertas, P., Calder, L.J., Garcia-Barreno, B., Melero, J. A., (2008). Structural properties of the human respiratory syncytial virus P protein: evidence for an elongated homotetrameric molecule that is the smallest orthologue within the family of paramyxovirus polymerase cofactors. *Proteins* **72**, 946–958.
40. Gilman, M.S.A., Liu, C., Fung, A., Behera, I., Jordan, P., Rigaux, P., Ysebaert, N., Tcherniuk, S., et al., (2019). Structure of the Respiratory Syncytial Virus Polymerase Complex. *Cell* **179** 193–204 e14.
41. Simabuco, F.M., Asara, J.M., Guerrero, M.C., Libermann, T.A., Zerbini, L.F., Ventura, A.M., (2011). Structural analysis of human respiratory syncytial virus p protein:

identification of intrinsically disordered domains. *Braz. J. Microbiol.* **42**, 340–345.
42. Noval, M.G., Esperante, S.A., Molina, I.G., Chemes, L.B., Prat-Gay, G., (2016). Intrinsic Disorder to Order Transitions in the Scaffold Phosphoprotein P from the Respiratory Syncytial Virus RNA Polymerase Complex. *Biochemistry* **55**, 1441–1454.
43. Pereira, N., Cardone, C., Lassoued, S., Galloux, M., Fix, J., Assrir, N., Lescop, E., Bontems, F., et al., (2017). New Insights into Structural Disorder in Human Respiratory Syncytial Virus Phosphoprotein and Implications for Binding of Protein Partners. *J. Biol. Chem.* **292**, 2120–2131.
44. Pretel, E., Sanchez, I.E., Fassolari, M., Chemes, L.B., de Prat-Gay, G., (2015). Conformational Heterogeneity Determined by Folding and Oligomer Assembly Routes of the Interferon Response Inhibitor NS1 Protein, Unique to Human Respiratory Syncytial Virus. *Biochemistry* **54**, 5136–5146.
45. Pretel, E., Camporeale, G., de Prat-Gay, G., (2013). The non-structural NS1 protein unique to respiratory syncytial virus: a two-state folding monomer in quasi-equilibrium with a stable spherical oligomer. *PLoS ONE* **8**, e74338.
46. Yang, M., Hay, J., Ruyechan, W.T., (2008). Varicella-zoster virus IE62 protein utilizes the human mediator complex in promoter activation. *J. Virol.* **82**, 12154–12163.
47. Sela, D., Chen, L., Martin-Brown, S., Washburn, M.P., Florens, L., Conaway, J.W., Conaway, R.C., (2012). Endoplasmic reticulum stress-responsive transcription factor ATF6alpha directs recruitment of the Mediator of RNA polymerase II transcription and multiple histone acetyltransferase complexes. *J. Biol. Chem.* **287**, 23035–23045.
48. Sela, D., Conkright, J.J., Chen, L., Gilmore, J., Washburn, M.P., Florens, L., Conaway, R.C., Conaway, J.W., (2013). Role for human mediator subunit MED25 in recruitment of mediator to promoters by endoplasmic reticulum stress-responsive transcription factor ATF6alpha. *J. Biol. Chem.* **288**, 26179–26187.
49. Haze, K., Yoshida, H., Yanagi, H., Yura, T., Mori, K., (1999). Mammalian transcription factor ATF6 is synthesized as a transmembrane protein and activated by proteolysis in response to endoplasmic reticulum stress. *Mol. Biol. Cell* **10**, 3787–3799.
50. Chen, X., Shen, J., Prywes, R., (2002). The luminal domain of ATF6 senses endoplasmic reticulum (ER) stress and causes translocation of ATF6 from the ER to the Golgi. *J. Biol. Chem.* **277**, 13045–13052.
51. Qiao, D., Skibba, M., Xu, X., Garofalo, R.P., Zhao, Y., Brasier, A.R., (2021). Paramyxovirus replication induces the Hexosamine Biosynthetic Pathway and Mesenchymal Transition via the IRE1a-XBP1s arm of the Unfolded Protein Response. *Am. J. Physiol. Lung Cell. Mol. Physiol.*. https://doi.org/10.1152/ajplung.00127.2021.
52. Smith, J.A., (2014). A new paradigm: innate immune sensing of viruses via the unfolded protein response. *Front. Microbiol.* **5**, 222.
53. Bourai, M., Lucas-Hourani, M., Gad, H.H., Drosten, C., Jacob, Y., Tafforeau, L., Cassonnet, P., Jones, L.M., et al., (2012). Mapping of Chikungunya virus interactions with host proteins identified nsP2 as a highly connected viral component. *J. Virol.* **86**, 3121–3134.
54. Solyom, Z., Schwarten, M., Geist, L., Konrat, R., Willbold, D., Brutscher, B., (2013). BEST-TROSY experiments for time-efficient sequential resonance assignment of large disordered proteins. *J. Biomol. NMR* **55**, 311–321.
55. Vranken, W.F., Boucher, W., Stevens, T.J., Fogh, R.H., Pajon, A., Llinas, M., Ulrich, E.L., Markley, J.L., et al., (2005). The CCPN data model for NMR spectroscopy: development of a software pipeline. *Proteins* **59**, 687–696.
56. Gouet, P., Robert, X., Courcelle, E., (2003). ESPript/ENDscript: Extracting and rendering sequence and 3D information from atomic structures of proteins. *Nucleic Acids Res.* **31**, 3320–3323.